NeuroImage 79 (2013) 129–137

Contents lists available at SciVerse ScienceDirect

NeuroImage

journal homepage: www.elsevier.com/locate/ynimg

Competing physiological pathways link individual differences in weight and abdominal adiposity to white matter microstructure

Timothy D. Verstynen [a,b,*], Andrea Weinstein [b,c,e], Kirk I. Erickson [b,c,e], Lei K. Sheu [d], Anna L. Marsland [c], Peter J. Gianaros [b,c,e]

[a] Department of Psychology, Carnegie Mellon University, USA
[b] Center for the Neural Basis of Cognition, Carnegie Mellon University, USA
[c] Department of Psychology, University of Pittsburgh, USA
[d] Department of Psychiatry, University of Pittsburgh, USA
[e] Center for the Neural Basis of Cognition, University of Pittsburgh, PA, USA

ARTICLE INFO

Article history:
Accepted 16 April 2013
Available online 29 April 2013

Keywords:
Adiposity
Inflammation
Obesity
Metabolic syndrome
White matter

ABSTRACT

Being overweight or obese is associated with reduced white matter integrity throughout the brain. It is not yet clear which physiological systems mediate the association between inter-individual variation in adiposity and white matter. We tested whether composite indicators of cardiovascular, lipid, glucose, and inflammatory factors would mediate the adiposity-related variation in white matter microstructure, measured with diffusion tensor imaging on a group of neurologically healthy adults (N = 155). A composite factor representing adiposity (comprised of body mass index and waist circumference) was associated with smaller fractional anisotropy and greater radial diffusivity throughout the brain, a pattern previously linked to myelin structure changes in non-human animal models. A similar global negative association was found for factors representing inflammation and, to a lesser extent, glucose regulation. In contrast, factors for blood pressure and dyslipidemia had positive associations with white matter in isolated brain regions. Taken together, these competing influences on the diffusion signal were significant mediators linking adiposity to white matter and explained up to fifty-percent of the adiposity–white matter variance. These results provide the first evidence for contrasting physiological pathways, a globally distributed immunity-linked negative component and a more localized vascular-linked positive component, that associate adiposity to individual differences in the microstructure of white matter tracts in otherwise healthy adults.

Introduction

Adiposity, a condition of excessive fat accumulation in the body, has emerged as a growing public health problem in the United States (Odgen and Carroll, 2010) and an emerging concern globally (Kelly et al., 2008). Increased accumulation of adipose tissue in the periphery of the body confers risk for changes in several metabolic and cardiovascular systems, including elevated blood pressure, dyslipidemia, insulin resistance, and systemic inflammation (Bastard et al., 2006; Johnson et al., 2012)—core features of the metabolic syndrome (Marsland et al., 2010). Yet elevated adiposity is also associated with impairments in cognitive function (Brogan et al., 2010, 2011; Brown and Thore, 2011; Horstmann et al., 2011; Nederkoorn et al., 2006; Yaffe, 2007; Yates et al., 2012) and with changes in both the structure and function of the central nervous system (Cazettes et al., 2011; García-García et al., 2012; Gianaros et al., in press; Haltia et al., 2007; Hendrick et al., 2011; Kullmann et al., 2011; Mueller et al., 2011; Portet et al., 2012; Segura et al., 2010; Stice et al., 2008; Verstynen et al., 2012; Walther et al., 2010; Yau et al., 2012). In particular, adiposity has been inversely related to multiple measures of white matter microstructure, as revealed by diffusion imaging methods (Gianaros et al., in press; Mueller et al., 2011; Stanek et al., 2011; Verstynen et al., 2012; Xu et al., 2011; Yau et al., 2012). Further evidence suggests that adiposity and obesity are associated with altered functional connectivity across brain regions (García-García et al., 2012; Kullmann et al., 2011), pointing to connectivity as a plausible neural basis for the altered cognitive function that occurs with elevated obesity.

While inherent differences in brain morphology and function may drive behaviors that increase adiposity, it is also possible that the adiposity-related alterations in peripheral physiological systems may lead to unfavorable changes in neural connectivity. In support of this hypothesis, many of the peripheral metabolic and vascular changes associated with increased adiposity have been linked, either directly or indirectly, to changes in measures of neural integrity (Fung et al., 2012;

* Corresponding author at: Carnegie Mellon University, Department of Psychology & Center for the Neural Basis of Cognition, 342u Baker Hall, Pittsburgh, PA 15213, USA. Fax: +1 412 624 9149.
E-mail address: timothyv@andrew.cmu.edu (T.D. Verstynen).

1053-8119/$ – see front matter © 2013 Elsevier Inc. All rights reserved.
http://dx.doi.org/10.1016/j.neuroimage.2013.04.075

Szczepanska-Sadowska et al., 2010; Thaler et al., 2012; Watson and Craft, 2006; Yates et al., 2012).

Accordingly, we set out to test the hypothesis that variation in obesity-linked physiological pathways mediates the relationship between adiposity and neural connectivity, measured at the level of white matter microstructure. Applying whole-brain mediation analyses on diffusion imaging measures of white matter microstructure, in a large sample of neurologically healthy adults, we evaluated two predictions. Based on prior findings (Gianaros et al., in press; Verstynen et al., 2012), we predicted that adiposity (body mass index, BMI, and waist circumference) would relate to lower fractional anisotropy (FA) scores through an increase in radial diffusivity (RD). Second, we tested whether adiposity–white matter relationships would be differentially mediated by variation in blood pressure (BP), dyslipidemia (circulating triglycerides and high-density lipoproteins), inflammation (C-reactive protein, CRP, and interleukin (IL)-6), and/or glucose control (fasting glucose and adiponectin). Characterizing such mediating pathways would provide novel insights into the mechanisms by which increased adiposity might influence neurocognitive health.

Materials & methods

Participants

Participants were 155 community-dwelling adults (78 men, 77 women; mean age = 40.7 ± 6.2 SD, range = 30–50 years) who were recruited via mass mailings to residents of Allegheny County, Pennsylvania (U.S.A.). All participants were screened for pre-existing health conditions. See Supplementary materials (Section 1.1) for a list of these criteria. Informed consent was obtained with approval of the University of Pittsburgh Institutional Review Board. The ethnicity of the sample was Caucasian (70.3%), African American (21.9%), Asian (5.8%), and multiracial/other (1.9%). Results of different analyses testing non-overlapping hypotheses on this diffusion imaging data set in relation to socioeconomic status have been reported elsewhere (Gianaros et al., in press).

Assessment of anthropometric and physiological variables

The primary measures collected for this study were:

(i) Waist circumference (an anthropometric indicator of relative adiposity, measured at end-expiration to the nearest 1/2 in. with a tape measure centered at the umbilicus) (M = 35.64, SD = 5.17 in., range = 25–48 in.).
(ii) Body mass index (BMI; weight in lb/(height in in.^{2}); M = 27.15, SD = 4.82, range = 18.5–42.3). There were 58 lean participants (BMI < 25), 57 overweight participants (25 < BMI < 30) and 40 obese participants (BMI > 30).
(iii) Seated, resting blood pressure (BP) was measured from the non-dominant arm with an oscillometric device (Critikon Dinamap 8100, Johnson & Johnson, Tampa, FL). Participants provided 3 BP measures taken 2 min apart after a ~20 min acclimation period, with the average of the last 2 of the 3 BP readings serving as the resting systolic (SBP) and diastolic (DBP) blood pressures (SBP, M = 121.44, STD = 9.48; DBP, M = 73.25, STD = 8.80).
(iv) Following an overnight fast, blood was drawn prior to magnetic resonance imaging (MRI) scanning. Serum was analyzed using a Synchron CX chemistry analyzer (Beckman-Coulter, Brea, CA) using reagents for glucose, triglyceride, high-density lipoprotein (HDL) and total cholesterol. Prior to analysis, measures of glucose (M = 88.21, STD = 12.81) and triglycerides (M = 81.07.10, STD = 16.49) were natural log transformed because of a skewed distribution. HDL measures (M = 49.88, STD = 16.48) were not transformed.
(v) Circulating levels of high-sensitivity CRP in mg/dL, were assayed on a SYNCHRON LX System (Beckman Coulter, Inc., Brea, California, with precision values of 5.0%CV within-run and 7.5%CV total for serum assays) in the Clinical Services Laboratory of the Department of Psychiatry at the University of Pittsburgh. Prior to analyses, CRP values (M = 0.28, SD = 0.47, range = 0.02 to 3.7) were natural log transformed because of a skewed distribution.
(vi) Interleukin-6 (IL-6) levels in pg/mL were determined using a high sensitivity quantitative sandwich enzyme immunoassay kit (R & D Systems). IL-6 levels were extrapolated from a standard curve with linear regression from a log-linear curve. All samples were run in duplicate and the average coefficient of variation (CV) between samples was <10%. Prior to analysis, IL-6 values (M = 1.79, STD = 1.84) were natural log transformed.
(vii) Adiponectin was measured using a radioimmunoassay procedure developed by Linco Research, Inc (see Supplementary materials, Section 1.2 for more information). Prior to analysis, adiponectin values (M = 12.61, STD = 7.03) were natural log transformed to adjust for skew.

Skew for each variable was determined using a QQ plot and significant skew determined when the r-squared comparison against a Gaussian distribution was less than 0.90.

Diffusion tensor imaging

All imaging was performed on a 3 Tesla Trio TIM whole-body MRI scanner (Siemens, Erlangen, Germany), equipped with a 12-channel phased-array head coil. Diffusion tensor imaging (DTI) was performed using a pair of pulsed-gradient, spin-echo sequences with a single-shot echo-planar imaging (EPI) readout. A parallel imaging algorithm (generalized auto-calibrating partial-parallel acquisition; GRAPPA) was applied during diffusion imaging to reduce echo-planar distortion. DTI parameters were: time-to-repetition (TR) = 5800 ms; time-to-inversion (TI) = 2500 ms; time-to-echo (TE) = 91 ms; flip angle = 90°; pixel size = 2 × 2 mm; resolution = 128 × 128 (with field-of-view [FOV] = 256 × 256 mm); 43 slices of 3 mm thickness with no gap; and total imaging time = 6 min and 19 s. Diffusion-sensitizing gradient encoding was applied in 30 uniform angular directions with a diffusion weighting of b = 1000 s/mm^2. A reference image with no diffusion gradient (b = 0) was also acquired. The acquisition sequence was repeated twice to improve the DTI signal-to-noise ratio.

All DTI data were processed using the FSL Diffusion Toolbox (v2.0; http://www.fmrib.ox.ac.uk/fsl/fdt/index.html), which encompassed the following steps: correction for motion and eddy current distortions by affine registration to the reference image, removal of skull and non-brain tissue, and calculation of diffusion parameters by fitting the diffusion images to a diffusion tensor model. The voxel-wise eigenvalues λ_1, λ_2, λ_3 and the eigenvectors of the diffusion tensor were computed from each participant's image. λ_1 corresponds to the largest eigenvalue reflecting water diffusivity parallel to the principle fiber direction (axial diffusivity, AD), and λ_2 and λ_3 correspond to perpendicular water diffusivity (radial diffusivity, RD). A weighted ratio of the standard deviation of these eigenvalues over the mean produces an estimate of fractional anisotropy (FA) in the voxel. FA is a common white matter measure derived from DTI, and it represents the 'shape' of the underlying water diffusion in each voxel. As barriers, like axons, neurofilaments, and myelin, restrict water movement water diffusion becomes more anisotropic (Hagmann et al., 2006). Hence, an FA value of 0 indicates perfectly spherical diffusion (i.e., no barriers), whereas an FA value of 1 indicates water that moves in a perfect line as constrained by surrounding barriers. In this way, larger FA values are assumed to reflect a greater 'integrity' of the barriers constraining the directional diffusion of water, although the direct relationship between

FA and underlying axonal integrity is still ambiguous (see Jones et al., 2013).

All FA images were normalized to the 1 × 1 × 1 mm MNI152 stereotaxic space via the FSL FA template (FMRIB58_FA). This was done by combining two transformations: (i) a nonlinear registration of each participant's FA image to the FMRIB59_FA template, and (ii) an affine transformation of the template to MNI152 space. These nonlinear and linear normalization parameters were then applied to the axial and radial diffusivity maps.

Analysis was performed both using a whole-brain cluster analysis and an isolated region of interest (ROI) approach. To determine the spatial distribution of FA associations, we identified clusters of voxels using an edge-based connectivity approach (Thurfjell et al., 1992). We corrected for multiple comparisons using a false-discovery-rate (Genovese et al., 2002) at the voxel-level-threshold of 0.05 and isolated consistent clusters at a spatial extent threshold of $k \geq 20$ contiguous voxels. ROIs were defined using an established atlas of a priori, anatomically defined white matter regions of interest (Mori et al., 2008). This atlas identifies 48 segments of core white matter pathways in both hemispheres. A list of the ROIs is shown in the Inline Supplementary Table S1.

Inline Supplementary Table S1 can be found online at http://dx.doi.org/10.1016/j.neuroimage.2013.04.075.

Indirect pathway analysis

Mediation analyses were performed by a regression approach with permutation based confidence interval estimation (Preacher and Hayes, 2008) using the Bootstrap Regression Analysis of Voxelwise Observations (BRAVO) toolbox (https://sites.google.com/site/bravotoolbox). Given previously reported effect sizes (Gianaros et al., in press; Mueller et al., 2011; Verstynen et al., 2012), our sample size afforded enough statistical power to apply a multiple mediator analysis to isolate indirect pathways linking changes in adiposity to variation in white matter microstructure (Mackinnon et al., 2002). All variables were z-scored prior to analysis, permitting a comparison of effect sizes across mediation models. Total path effects (c paths) were modeled using ordinary least squares regressions of FA values on each component variable, after controlling for age, sex and education (i.e., by a similar model as in Eq. (3) below, but without mediation terms). Direct path effects (c' paths) were modeled as the association of a given the Adiposity latent variable with FA values, after controlling for age, sex, education and mediator variables corresponding to the indirect paths. Indirect path effects were modeled as the product of the association of the Adiposity latent variable (a paths) with the mediating variables and the associations of the mediating variables with FA values (b paths). All potential mediating pathways were evaluated simultaneously in a single regression model (i.e., multiple mediator modeling).

The parameters *a, b and c′* were determined by the following ordinary least squares regression models

$$\mathbf{M} = a\mathbf{X}_{\text{Adiposity}} + \phi_1\mathbf{C}_{\text{Age}} + \phi_2\mathbf{C}_{\text{Sex}} + \phi_3\mathbf{C}_{\text{Education}} + \eta \quad (1)$$

$$\mathbf{Y}_{\text{FA}} = c'\mathbf{X}_{\text{Adiposity}} + bM + \phi_1\mathbf{C}_{\text{Age}} + \phi_2\mathbf{C}_{\text{Sex}} + \phi_3\mathbf{C}_{\text{Education}} + \eta \quad (2)$$

where $\mathbf{Y}_{\text{FA}}$ is the $n \times 1$ vector of FA values, n is the number of subjects with viable FA images ($N = 145$, see below) and η reflects noise in the model. $\mathbf{M}$ is the $n \times m$ vector of mediator variables, where m is the number of mediating factors being evaluated. When $m > 1$, $\mathbf{M}$ is a matrix and thus the first equation is a multivariate regression problem wherein b becomes a $1 \times m$ vector instead of a scalar value. The vectors $\mathbf{C}_{\text{Age}}$, $\mathbf{C}_{\text{Sex}}$ and $\mathbf{C}_{\text{Education}}$ are nuisance covariates, with effect sizes f_1, f_2 and f_3 respectively, and η is the residual error in each model. The strength of the indirect pathway is determined as the product of the a and b coefficients (i.e., $a * b$).

A permutation approach was used to evaluate the statistical confidence and significance of the direct and indirect pathways at each voxel (Preacher and Hayes, 2008). For each iteration of the algorithm, the values in the variable vectors ($\mathbf{X}_{\text{Adiposity}}$, $\mathbf{Y}_{\text{FA}}$, and $\mathbf{M}$) were scrambled independently. The values for a, b, c' and $a * b$ from these permuted models were stored in a separate matrix, and this process was repeated for 500 iterations per voxel. The significance of the direct and indirect paths was determined from the distribution of bootstrapped values using a bias-corrected and accelerated method (Diciccio and Efron, 1996) at a one-tailed criterion of 0.025.

In order to estimate the probability of observing spurious significant pathways (i.e., Type-I error rate), we ran a set of simulated mediation models where the dependent and mediator variables were random noise vectors. For the total pathway analysis, we generated an $n \times 1$ random independent vector ($\mathbf{X}_{\text{sim}}$), where n is the number of subjects, that was drawn from a standard normal distribution and was selected so as not to be correlated with any of the components (maximum allowed $r = 0.025$). We then used this $\mathbf{X}_{\text{sim}}$ variable to regress on whole-brain FA maps as described above, including controlling for age, sex and education. For the mediation pathway analysis, the dependent variable was left as the $X_{\text{Adiposity}}$ and an $n \times 4$ matrix, $\mathbf{M}_{\text{sim}}$, was generated from a standard normal distribution to replace the mediating factors. As with $\mathbf{X}_{\text{sim}}$, each column in $\mathbf{M}_{\text{sim}}$ was selected so as to not be correlated with any of the potential mediators. Both the simulated total pathway and mediation pathway analyses were repeated 20 times in order to generate 95% confidence intervals of the whole-brain distribution of model parameters (c, c', a, b, & $a * b$) based on chance. The confidence interval range was adjusted to account for multiple comparisons such that

$$95\%\text{CI} = \mu \pm \Phi\left(1-\alpha^{1/n}\right)\sigma/\sqrt{n} \quad (3)$$

where μ is the mean correlation across voxels for the random noise model, σ is the variance, n is the number of comparisons in the set (i.e., 5 for total pathway comparisons, 4 for mediation pathways) and $a = 0.05$. This adjusted interval provides a chance detection rate for the whole-brain analyses.

For these analyses, white matter voxels were selected from the raw DTI images by identifying voxels with FA values greater than 0.3 to increase the likelihood of excluding gray matter voxels, and only data from the smoothed FA maps were used for mediation regression analyses (4 mm full-width half-maximum smoothing kernel). This smoothing kernel was used in order to accommodate for coregistration errors in the FA normalization process as well as meet the assumptions of Gaussian noise in the spatial statistical analysis. Processing and analysis were performed iteratively for each white matter voxel and began by extracting FA values for each participant.

Finally, to quantify chance expectation in both the total and mediation pathway analysis, we modeled a set of simulated experiments where the inputs and mediators are random noise terms (i.e., null-effect simulations). All confidence intervals of chance detection rates were adjusted for multiple comparisons (Supplementary methods, Section 1.3).

Results

Adiposity-linked physiological pathways

Given the large number of anthropometric and physiological measures collected, we first applied a latent variable analysis to derive a smaller number of five composite factors: Adiposity, BP, Dyslipidemia, Inflammation, and Glucose regulation. Each latent variable was created using principal component analysis (PCA; *princomp.m* in Matlab) to isolate the dominant source of shared variance between the component

Table 1
Correlations between the PCA component factors. Asterisks indicate $p < 0.025$ (*) or $p < 0.001$ (**), determined using a bootstrap permutation test.

	BP	Dyslipidemia	Inflammation	Glucose
Adiposity	0.43**	0.56**	0.51**	0.35**
BP		0.36**	0.26**	0.21*
Dyslipidemia			0.28**	0.52**
Inflammation				0.18*

variables. This orthogonalizes the variance from the component variables but allows for comparison of relationships between PCA-derived components. The Adiposity component was generated using BMI and waist circumference, and accounted for 91.02% of the shared variance between BMI and waist circumference. While BMI and waist circumference are indirect measures of adiposity, this PCA-derived Adiposity component identifies the shared variance between these two measures that reflects adiposity-related, unhealthy weight gain. Remaining component measures were ordered so that they positively correlated with the Adiposity component. The BP component was generated using systolic BP and diastolic BP and accounted for 86.02% of the shared variance. The Dyslipidemia component was generated from the high-density lipoprotein and log transformed triglyceride variables, which explained 75.59% of the shared variance. The Inflammation component was a composite of the log-transformed versions of the CRP and IL-6 variables and explained 77.38% of the shared variance. Finally the Glucose component was generated from the log transform of the fasting glucose and adiponectin measures, with 65.14% of the shared variance explained by the principal component.

Higher scores on the Adiposity factor were associated with older age ($r = 0.32$, $p = 0.035$) and fewer years of education ($r = -0.20$, $p = 0.007$). Using a logistic regression model, we failed to detect a significant relationship between Adiposity and gender ($\beta = -0.02$, $p = 0.21$). Table 1 shows the correlations between each of the component variables. Adiposity was significantly correlated with all four physiological factors. Within the potential mediators, we found moderate and positive correlations. Of these inter-variable correlations, only the correlation between the inflammation and glucose components failed to pass significance threshold based on a Bonferroni correction for 6 comparisons (corrected $p = 0.0085$).

Adiposity and white matter microstructure

Our analysis focused on the whole-brain pattern of anthropometric and physiological system effects in the brain. Therefore the distribution of voxel coefficients across the entire brain was used as our key measure of interest, rather than focusing on specific clusters of regions. Similar to previous reports (Gianaros et al., in press; Verstynen et al., 2012), there was a predominantly negative Adiposity–FA association across the white matter voxels, after controlling for age, sex and education. This effect is expressed as a leftward shift in distribution of correlations across all white matter voxels, compared to the expectations of chance generated using the bootstrap test (Fig. 1a). As a measure of this global effect, we computed the percentage of significant ($p < 0.025$) positive and negative voxels (Table 2). Consistent with previous observations (Gianaros et al., in press; Mueller et al., 2011; Stanek et al., 2011; Verstynen et al., 2012; Xu et al., 2011; Yau et al., 2012), we found more voxels with significant negative Adiposity–FA correlations than would be expected by chance (1925 voxels versus 1832 upper bound expected from the randomized simulations). Only the radial diffusivity (RD) component of the diffusion signal correlated with differences in the Adiposity variable in these negative voxels (Table 2). Interestingly, there were fewer voxels with positive associations than would be predicted by chance, consistent with a global negative shift in FA values with higher levels of adiposity. As with the negatively associated voxels, in positively associated voxels only RD was correlated with the Adiposity factor.

Voxels with significant Adiposity correlations were generally clustered in well-defined, and often, bilateral regions (Fig. 2a). Of the 48 a priori white matter ROIs tested (see Materials & methods), 6 had more significant negative voxels than expected by chance: the genu of the corpus callosum, the left inferior cerebellar peduncle, the left and right superior cerebellar peduncle, and the left and right anterior segments of the corona radiata (Inline Supplementary Table S1).

Physiology-white matter relationships

Unlike Adiposity, the BP latent variable did not show a global shift in the distribution of BP–FA correlations (Fig. 1b). While the mode of this distribution overlapped zero, we found slightly more positive voxels than expected by chance (1640 voxels); however, the rate of significant

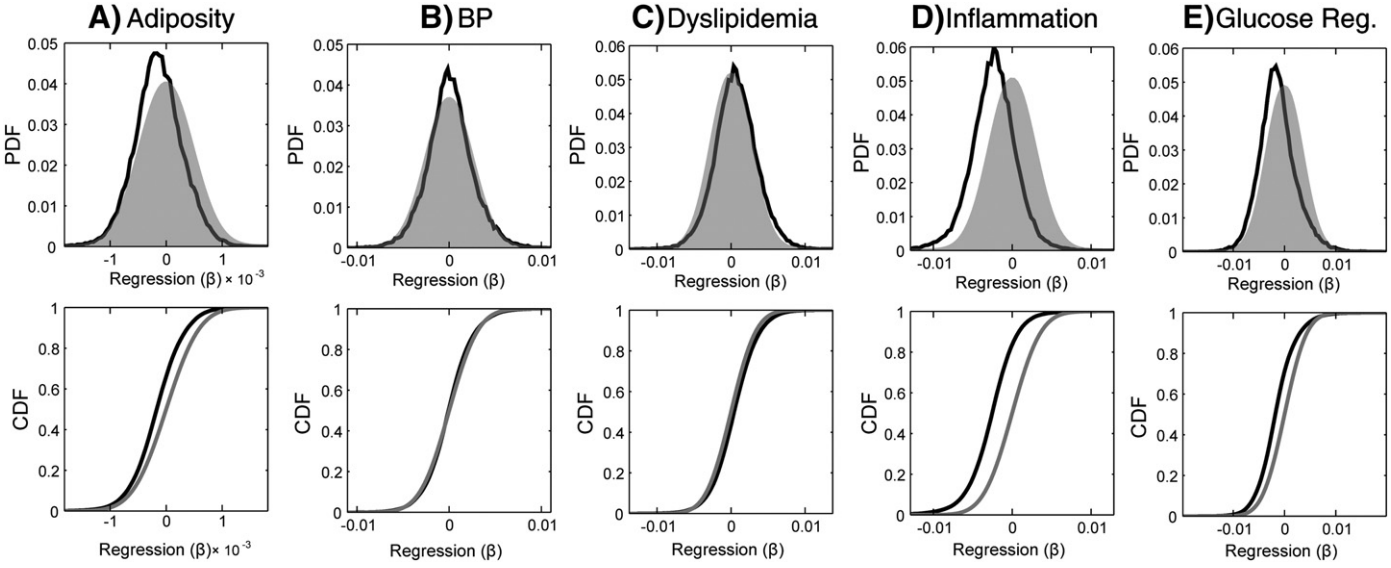

Fig. 1. Global distributions of the regression coefficients showing the relationship between each latent variable and fractional anisotropy (FA) across all white matter voxels. Black distributions show the observed values. Gray distributions show the estimated null distribution determined from bootstrapped simulations. PDF, probability density function; CDF, cumulative distribution function.

Table 2
Global white matter associations. Asterisks indicate where the percentage of significant FA associations falls outside the bounds of the 95% confidence interval (CI) estimated from the random simulations (bounds shown in column section labels). Relations to axial (AD) and radial (RD) diffusivity for the voxels with significant FA associations are shown in the adjacent columns.

	Positive effects (95% CI = 0.86%–2.70%)					Negative effects (95% CI = 1.08%–3.36%)				
	% Sig.	AD Cxy	p value	RD Cxy	p value	% Sig	AD Cxy	p value	RD Cxy	p value
Adiposity	0.53*	−0.04	0.652	−0.34	0.000	3.53*	−0.16	0.052	0.25	0.008
BP	3.01*	0.18	0.026	−0.31	0.000	1.56	−0.16	0.050	0.23	0.002
Dyslipidemia	5.51*	0.10	0.236	−0.31	0.000	1.38	−0.17	0.028	0.21	0.024
Inflammation	0.27*	0.11	0.238	−0.31	0.000	13.54*	−0.18	0.066	0.24	0.010
Glucose	1.64	0.36	0.000	−0.20	0.058	6.55*	−0.09	0.392	0.38	0.002

negative voxels fell within the 95% confidence interval of chance (Table 2). Within the positive clusters, both the axial and radial components of diffusivity correlated with BP (Table 2). These clusters were distributed across white matter voxels, with the largest found bilaterally in the internal and external capsules (Fig. 2b). Out of 48 ROIs, 19 had more significant positive voxels than expected by chance (based on the 95% confidence interval from random model simulations) (Inline Supplementary Table S1).

The Dyslipidemia factor had similar white matter effects as BP. The overall distribution of Dyslipidemia–FA associations had a mean near zero and overlapped with the distribution of chance estimated from the bootstrap simulations (Fig. 1c). However, there was a slightly longer tail on the positive end of the distribution, with more significant positive voxels than expected by chance (3007 voxels; Table 2). Unlike BP, however, only the radial component of the diffusivity signal correlated with the Dyslipidemia factor in these positive voxels (Table 2). The positively associated voxels were distributed throughout the brain, but heavily clustered in regions containing corona radiata projections (Fig. 2c). Far more ROIs showed significant positive associations with Dyslipidemia, 30/48, than were found with BP (Inline Supplementary Table S1).

The Inflammation factor had a similar association to white matter as Adiposity, with the distribution of FA correlations being shifted in a negative direction (Fig. 1d). Inflammation had the largest rate of significant voxels out of all the components tested, with over 13% (7385 voxels) of the white matter voxels having a significant negative association with Inflammation (Table 2), over four times the upper bound of the adjusted 95% confidence interval of chance (3.36% of voxels). In these voxels with negative associations, Inflammation was also associated with a change in the radial, but not axial, component of the diffusion signal. As with Adiposity, the detection rate of negative Inflammation–FA associations fell below the lower bound of the confidence interval from chance, consistent with a global shift in FA with increased Inflammation. The clusters of negative voxels were distributed throughout the brain (Fig. 2d), with 37 out of 48 ROIs showing significant negative associations with Inflammation (Inline Supplementary Table S1).

The Glucose regulation factor showed a similar, albeit weaker, negative association with FA as Inflammation (Fig. 1e). Nearly twice as many voxels had significant negative associations (3574 voxels) than expected by chance from the random simulations (Table 2). In these negative voxels, only changes in radial diffusivity correlated with the Glucose factor. Similar to Inflammation, the significant clusters were distributed throughout most of the white matter voxels (Fig. 2e), with 33/48 ROIs showing more significant negative voxels than expected by chance (Inline Supplementary Table S1). While there were a few dense clusters of significant positive FA associations, particularly in the corona radiata, the overall number of voxels with significant positive associations was not outside the confidence intervals of chance.

In general there was a modest degree of overlap of the expression of the anthropometric and physiological effects on FA. These are summarized in the Supplementary Materials (Supplementary Results, Section 2.1).

Mediating pathways between adiposity and white matter

To determine indirect mediating pathways between Adiposity and white matter (i.e., Adiposity to physiological system to FA), we adopted a permutation analysis approach (Preacher and Hayes, 2008). Our first goal was to determine the chance detection rates in a set of 20 simulated experiments where the mediating variables had no correlation with Adiposity or the four physiological factors (see Materials & methods). Out of 80 simulated indirect pathways, the upper bound of the 95% confidence interval for detecting a spuriously significant voxel was 26.28%, after a Bonferroni correction for multiple comparisons.

All four physiological factors had more voxels with significant indirect pathways than would be expected by chance (Fig. 3a). The largest number of indirect pathway voxels was the Inflammation factor, followed by the Dyslipidemia, BP, and Glucose factors. In general, clusters of significant voxels were distributed throughout the white matter voxels in regions similar to those found in the original physiology–FA regressions (see Fig. 4). Fig. 5 shows histograms of the indirect pathways for all four physiological factors. Subset histograms show the distribution of statistically significant positive (red) and negative (blue) voxels. Both the BP and Dyslipidemia factors had a higher ratio of positive effects, with an overall global shift in the distribution of coefficients in a positive direction. There were 50% more positive voxels in the BP distribution (33.82% positive vs. 22.47% negative) and 245% more in the Dyslipidemia distribution (55.57% positive vs. 16.12% negative). In contrast, Inflammation had a very strong negative shift in the indirect pathway ($a * b$) coefficients, with nearly six times as many negative voxels (69.04% of voxels) as positive (10.95%). Finally, the Glucose regulation factor had a fairly equal distribution of positive (28.11%) and negative (23.98%) effects.

These indirect pathways can only be considered statistical mediators when both the indirect pathway and the original physiological–FA effects are both significant in the same voxel (given that Adiposity is also correlated with each physiological factor). Based on the random simulation models, there is a chance of seeing this happen spuriously in a maximum of 2.3% of white matter voxels. We found much higher detection rates for all four physiological factors. Inflammation had the greatest detection rates with 13.8% of all white matter voxels being significant, followed by the Glucose (6.7%), Dyslipidemia (6.5%) and BP (4.4%) factors. The location of these mediating voxels overlapped nearly perfectly with the location of the original correlation results for each physiological pathway (see Fig. 2): BP (96.6% overlap), Dyslipidemia (94.7%), Inflammation (99.9%) and Glucose (82.4%).

The Inflammation effects are especially interesting in their spatial similarity to the original Adiposity effects. A vast majority (97%) of the voxels with significant Inflammation–FA relationships (Fig. 2d) were also mediators for Adiposity–FA effects. We elaborate on the relevance of this overlap in the Discussion.

Competing influences on white matter

The direction of the relationships between each physiological factor and FA suggests that they exert competing effects on the underlying

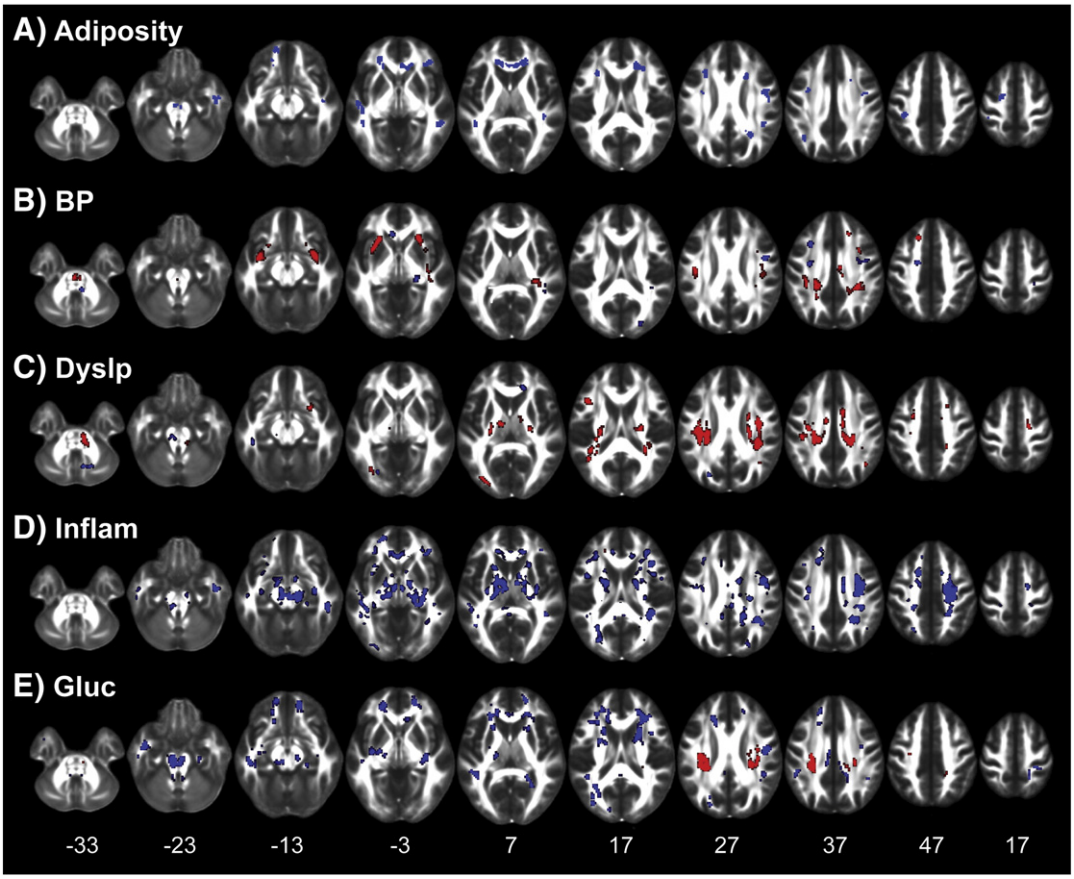

Fig. 2. The spatial distribution of positive (red voxels) and negative (blue voxels) associations between each latent variable and FA. Clusters are thresholded to a minimum of 20 connected voxels and a cluster-wise false discovery rate of 0.05. The z-plane coordinates of each slice, in MNI space, are presented at the bottom. A) Adiposity; B) BP, Blood Pressure factor; C) Dyslp, Dyslipidemia factor; D) Inflam, Inflammation factor; E) Gluc, Glucose regulation factor.

white matter signal, with some relating to higher FA and others (i.e., Inflammation) lower FA. Since Adiposity is positively correlated with all the physiological variables, it suggests that the original regression results between Adiposity and FA, called the total pathway, may be weaker due to these competing influences on FA. By including these indirect pathways in the mediation model, we can control for these countermanding effects in the estimate of the direct (c') pathway, which is the relationship between Adiposity and FA after controlling for the physiological mediators. Consistent with this interpretation, we detected nearly eight times as many significant positive c' voxels (4.01%; 95% CI UB = 1.03%) and fifty percent more negative voxels (5.31%; 95% CI UB = 3.98%) than were detected in the original total (c) pathway analysis.

Because controlling for the underlying physiological factors improved detection of significant Adiposity–FA relationships, we next

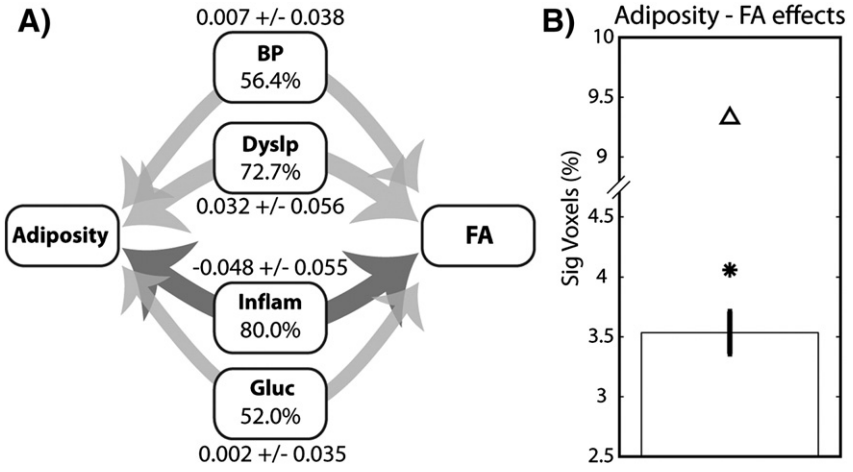

Fig. 3. A) Illustration of the indirect pathway analysis for all four factors tested. Percentages show the number of voxels with statistically significant ($p < 0.025$) indirect pathways, and depicted by the weight of the arrows. Light gray arrows show average positive effects, while dark gray shows average negative effects. The upper bound of the chance 95% confidence interval is 26.54%. The mean and standard deviation for the indirect pathway coefficients is shown adjacent to each pathway label. Same factor labels as Fig. 2. B) Percent of voxels with significant Adiposity–FA associations. Error bars show 95% confidence interval from 20 random simulations, followed by the detection rate for the original regression model (*) and the direct pathway model (Δ) after accounting for the indirect physiological pathways.

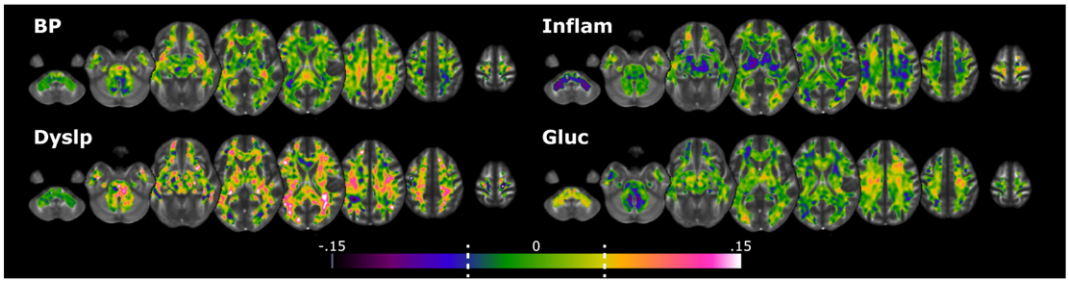

Fig. 4. Distribution of indirect pathways coefficients. Dashed lines on the color bars show the median coefficient values for significant positive and negative effects. Labeling conventions are the same as Fig. 2.

determined how influential each indirect pathway was on the change in the Adiposity–FA coefficients. We calculated the difference between the total (c) and direct (c') Adiposity–FA pathways. This vector of difference scores was then subjected to a regression analysis where the indirect pathway coefficients for each physiological variable were included as independent variables. Accounting for all indirect pathways explained 49.69% of the variance in the change in Adiposity–FA relationship across all white matter voxels. Follow up analyses for each pathway separately revealed that BP regulation explained the most variance (12.58%), followed by Dyslipidemia (7.93%), Inflammation (6.59%) and Glucose (1.71%).

Discussion

In a healthy cross-sectional sample of adults, we confirmed that higher levels of adiposity associate with a global decrease in FA throughout the brain that appears to occur predominantly through an increase in radial diffusivity (Gianaros et al., in press; Mueller et al., 2011; Stanek et al., 2011; Verstynen et al., 2012; Xu et al., 2011; Yau et al., 2012). We also report the novel finding that four simultaneously measured physiological systems associated with increased adiposity showed a mixture of numerically positive and negative influences on the white mater signal, with much stronger effect sizes than the anthropometric adiposity measure. The latent variables reflecting systemic inflammation and glucose regulation most strongly resembled the pattern of effects seen with the adiposity factor. In contrast, the latent variables for blood pressure and dyslipidemia were strongly and positively correlated with FA, but this effect was isolated in specific clusters rather than globally expressed throughout the brain.

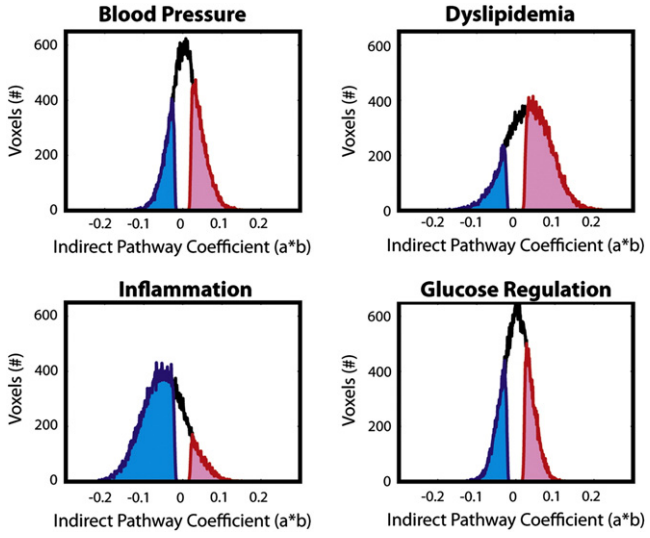

Fig. 5. Distributions of indirect pathway coefficients across all white matter voxels. Black distributions show across all voxels. Blue distributions show voxels with significant ($p < 0.025$, bootstrapped) negative effects, while red distributions show significant positive effects.

More importantly, here we report for the first time that several peripheral physiological systems serve as mediating pathways for the relationship between elevated adiposity and white matter structure. There were significantly more voxels with indirect pathways than predicted by chance for all four physiological systems. However, rather than being uniformly expressed, we find that the physiological mediators may interact in opposing ways. Consistent with this interpretation, we found that: (a) the extent and direction of total physiological effects on FA across the white matter voxels varied, (b) accounting for physiological factors in the mediation model resulted in more significant Adiposity–FA relationships than expected by chance, and (c) including all four mediating pathways accounted for nearly 50% of the change between the total and direct Adiposity–FA pathways.

Our results highlight two possible neurobiological routes by which variation in physiological systems may influence the morphology of the underlying white matter pathways. First, there is a strong global negative pattern that is distributed throughout the white matter voxels and loads heavily onto systemic inflammation (see also Gianaros et al., in press) and partially onto glucose regulation. Factors linked to this global signal change are correlated with changes in the radial diffusivity component of the DTI signal, resembling patterns seen in the diffusion signal of animal models of demylenation (Budde et al., 2009; Song et al., 2005). Physiologically this pattern may reflect a common peripheral molecular system that adversely impacts the central nervous system (for full review, see (Rosano et al. (2012). Central adipose tissue, particularly white adipose tissue, is a source of pro-inflammatory cytokines, such as IL-6, IL-1β, and tumor necrosis factor (TNF)-α. In the periphery, these cytokines stimulate production of CRP and fibrinogen. In animal models, over expression of TNF-α with obesity is linked to increased insulin resistance (Barzilay et al., 2001; Hotamisligil et al., 1993), which is one possible mechanism that explains why obese animals with elevated circulating CRP levels have a two-fold increase for developing Type-II diabetes (Uysal et al., 1997). In the central nervous system, both the pro-inflammatory cytokines and insulin are believed to influence cell integrity by introducing a local inflammatory response in the microglia (Rosano et al., 2012). In this way, the global negative signal change may reflect a distributed, immunity-linked influence on myelin morphology itself, which may have secondary implications for neural function.

The second pattern reflects localized variation in the diffusion signal linked to vascular physiological factors, including blood pressure, dyslipidemia, and, to a smaller extent, insulin systems. This local signal change is manifested as an increase in FA, with non-specific associations to both axial and radial diffusivity. At this point, it is difficult to interpret the neurobiological implications of this pattern of results. In animal models, vascular insults, such as microscopic ischemic damage from lacunar strokes, correlate with changes in both the axial and radial diffusivity components (Boretius et al., 2012; Wang et al., 2008); however, the direction of these changes is opposite to what we detected here (i.e., FA and axial diffusivity decrease, radial diffusivity increases).

Also, the positive FA associations with BP, dyslipidemia, and glucose control all fall in roughly the same area of the white matter (see Figs. 2b, c, and e), along the corona radiata near the intersection of several crossing pathways. Given the fiber crossings in this area, it is possible that underlying axonal integrity is reducing with these factors, but the simplicity of the single tensor model cannot adequately capture the nature of these changes. Future studies with more sophisticated models of the underlying diffusion patterns, such as orientation distribution functions (Wedeen et al., 2005), may be able to better resolve this odd pattern of FA associations.

When interpreting the underlying differences in white matter morphology, it is important to keep in mind that our sample was a generally healthy segment of the population. Thus the patterns we tested reflects natural, sub-clinical variation in white matter microstructure, rather than pathological white matter damage, and are not confounded by secondary factors related to pathological disease states. The bimodal pattern of global inflammation-linked drops in FA and localized vascular-linked increases in FA is in agreement with the recent prediction that both metabolic and cardiovascular systems may influence the central nervous system through mechanisms that depend on neurovascular integrity (Fung et al., 2012). Although, it should be pointed out that 50% of the variance in the adiposity–FA relationship is yet unaccounted for, suggesting additional mediating mechanisms may yet account for obesity and white matter relationships. Nonetheless, understanding the functional implications of these different associations should be a goal of future work.

Finally, the inherent limitations of a cross-sectional design restrict our ability to infer the directionality of these anthropometric, physiological and white matter relationships. In humans this can be achieved through longitudinal studies using targeted interventions for obesity, such as exercise or pharmacological studies, where direct changes in peripheral mechanisms can be mapped to changes in white matter architecture and subsequent cognitive and behavioral outcomes.

Supplementary data to this article can be found online at http://dx.doi.org/10.1016/j.neuroimage.2013.04.075.

Acknowledgments

TV & PG were supported by NIH Grant R01-HL089850-05. KIE was supported by a Junior Scholar Award from the Pittsburgh Claude D Pepper Older Americans Independence Center (P30 AG024827) and the University of Pittsburgh Alzheimer's Disease Research Center (P50 AG005133). TV & PG contributed equally to this work.

Conflict of interest statement

None of the authors report any conflicts of interest.

References

Barzilay, J., Abraham, L., Heckbert, S., Cushman, M., Kuller, L., Resnick, H., Tracy, R., 2001. The relation of markers of inflammation to the development of glucose disorders in the elderly: the Cardiovascular Health Study. Diabetes 50, 2384–2389.

Bastard, J.-P., Maachi, M., Lagathu, C., Kim, M.J., Caron, M., Vidal, H., Capeau, J., Feve, B., 2006. Recent advances in the relationship between obesity, inflammation, and insulin resistance. Eur. Cytokine Netw. 17, 4–12.

Boretius, S., Escher, A., Dallenga, T., Wrzos, C., Tammer, R., Brück, W., Nessler, S., Frahm, J., Stadelmann, C., 2012. Assessment of lesion pathology in a new animal model of MS by multiparametric MRI and DTI. Neuroimage 59, 2678–2688.

Brogan, A., Hevey, D., Pignatti, R., 2010. Anorexia, bulimia, and obesity: shared decision making deficits on the Iowa Gambling Task (IGT). J. Int. Neuropsychol. Soc. 16, 711–715.

Brogan, A., Hevey, D., O'Callaghan, G., Yoder, R., O'Shea, D., 2011. Impaired decision making among morbidly obese adults. J. Psychosom. Res. 70, 189–196.

Brown, W., Thore, C.R., 2011. Cerebral microvascular pathology in aging and neurodegeneration. Neuropathol. Appl. Neurobiol. 37, 56–74.

Budde, M.D., Xie, M., Cross, A.H., Song, S., 2009. Axial diffusivity is the primary correlate of axonal injury in the experimental autoimmune encephalomyelitis spinal cord: a quantitative pixelwise analysis. J. Neurosci. 29, 2805–2813.

Cazettes, F., Cohen, J., Yau, P.L., Talbotc, H., Convit, A., 2011. Obesity-mediated inflammation may damage the brain circuit that regulates food intake. Brain Res. 7565, 101–109.

Dicicciio, T.J., Efron, B., 1996. Bootstrap confidence intervals. Stat. Sci. 11, 189–228.

Fung, A., Vizcaychipi, M., Lloyd, D., Wan, Y., Ma, D., 2012. Central nervous system inflammation in disease related conditions: mechanistic prospects. Brain Res. 1446, 144–155.

García-García, I., Jurado, M.Á., Garolera, M., Segura, B., Sala-Llonch, R., Marqués-Iturria, I., Pueyo, R., Sender-Palacios, M.J., Vernet-Vernet, M., Narberhaus, A., Ariza, M., Junqué, C., 2012. Alterations of the salience network in obesity: a resting-state fMRI study. Hum. Brain Mapp. http://dx.doi.org/10.1002/hbm.22104 (Apr 21, Electronic publication ahead of print).

Genovese, R., Lazar, N., Nichols, T., 2002. Thresholding of statistical maps in functional neuroimaging using the false discovery rate. Neuroimage 15, 870–878.

Gianaros, P.J., Marsland, A.L., Sheu, L.K., Erickson, K.I., Verstynen, T.D., 2012. Inflammatory, pathways link socioeconomic inequalities to white matter architecture. Cereb. Cortex. PubMed PMID: 22772650 (Jul 6 (in press), Electronic publication ahead of print).

Hagmann, P., Jonasson, L., Maeder, P., Thiran, J., Wedeen, V.J., Meuli, R., 2006. Understanding diffusion MR imaging techniques : from scalar diffusion-weighted imaging to diffusion tensor imaging and byeon. Radiographics 26, S205–S224.

Haltia, L.T., Viljanen, A., Parkkola, R., Kemppainen, N., Rinne, J.O., Nuutila, P., Kaasinen, V., 2007. Brain white matter expansion in human obesity and the recovering effect of dieting. J. Clin. Endocrinol. Metab. 92, 3278–3284.

Hendrick, O.M., Luo, X., Zhang, S., Li, C.-S.R., 2011. Saliency processing and obesity: a preliminary imaging study of the stop signal task. Obesity 1–7.

Horstmann, A., Busse, F.P., Mathar, D., Müller, K., Lepsien, J., Schlögl, H., Kabisch, S., Kratzsch, J., Neumann, J., Stumvoll, M., Villringer, A., Pleger, B., 2011. Obesity-related differences between women and men in brain structure and goal-directed behavior. Front. Hum. Neurosci. 5, 58.

Hotamisligil, G., Shargill, N., Spiegelman, B., 1993. Adipose expression of tumor necrosis factor-alpha: direct role in obesity-linked insulin resistance. Science 259, 87–91.

Johnson, A.R., Milner, J.J., Makowski, L., 2012. The inflammation highway: metabolism accelerates inflammatory traffic in obesity. Immunol. Rev. 249, 218–238.

Jones, D.K., Knösche, T.R., Turner, R., 2013. White matter integrity, fiber count, and other fallacies: the do's and don'ts of diffusion MRI. Neuroimage 73, 239–254.

Kelly, T., Yang, W., Chen, C.-S., Reynolds, K., He, J., 2008. Global burden of obesity in 2005 and projections to 2030. Int. J. Obes. 32, 1431–1437 (2005).

Kullmann, S., Heni, M., Veit, R., Ketterer, C., Schick, F., Häring, H.-U., Fritsche, A., Preissl, H., 2011. The obese brain: Association of body mass index and insulin sensitivity with resting state network functional connectivity. Hum. Brain Mapp. 1061, 1052–1061.

Mackinnon, D.P., Lockwood, C.M., Hoffman, J.M., West, S.G., Sheets, V., 2002. A comparison of methods to test mediation and other intervening variable effects. Psychol. Methods 7, 1–35.

Marsland, A.L., McCaffery, J.M., Muldoon, M.F., Manuck, S.B., 2010. Systemic inflammation and the metabolic syndrome among middle-aged community volunteers. Metabolism 59, 1801–1808.

Mori, S., Oishi, K., Jiang, H., Jiang, L., Li, X., Akhter, K., Hua, K., Faria, A.V., Mahmood, A., Woods, R., Toga, A.W., Pike, G.B., Neto, P.R., Evans, A., Zhang, J., Huang, H., Miller, M.I., Van Zijl, P., Mazziotta, J., 2008. Stereotaxic white matter atlas based on diffusion tensor imaging in an ICBM template. Neuroimage 40, 570–582.

Mueller, K., Anwander, A., Möller, H.E., Horstmann, A., Lepsien, J., Busse, F., Mohammadi, S., Schroeter, M.L., Stumvoll, M., Villringer, A., Pleger, B., 2011. Sex-dependent influences of obesity on cerebral white matter investigated by diffusion-tensor imaging. PLoS One 6, e18544.

Nederkoorn, C., Braet, C., Van Eijs, Y., Tanghe, A., Jansen, A., 2006. Why obese children cannot resist food: the role of impulsivity. Eat. Behav. 7, 315–322.

Odgen, C., Carroll, M., 2010. Prevelance of overweight, obesity, and extreme obesity among adults: United States, trends 1976–1980 through 2007–2008.

Portet, F., Brickman, A.M., Stern, Y., Scarmeas, N., Muraskin, J., Provenzano, F.A., Berr, C., Bonafé, A., Artero, S., Ritchie, K., Akbaraly, T.N., 2012. Metabolic syndrome and localization of white matter hyperintensities in the elderly population. Alzheimers Dement. 8, S88–S95.e1.

Preacher, K., Hayes, A., 2008. Asymptotic and resampling strategies for assessing and comparing indirect effects in multiple mediator models. Behav. Res. Methods 40, 879–891.

Rosano, C., Marsland, A.L., Gianaros, P.J., 2012. Maintaining brain health by monitoring inflammatory processes: a mechanism to promote successful aging. Aging Dis. 3, 16–33.

Segura, B., Jurado, M.A., Freixenet, N., Bargalló, N., Junqué, C., Arboix, A., 2010. White matter fractional anisotropy is related to processing speed in metabolic syndrome patients: a case-control study. BMC Neurol. 10, 64.

Song, S., Yoshino, T.J., Le, T.Q., Lin, S., Sun, S., Cross, A.H., Armstrong, R.C., 2005. Demyelination increases radial diffusivity in corpus callosum of mouse brain. Neuroimage 26, 132–140.

Stanek, K.M., Grieve, S.M., Brickman, A.M., Korgaonkar, M.S., Paul, R.H., Cohen, R.A., Gunstad, J.J., 2011. Obesity is associated with reduced white matter integrity in otherwise healthy adults. Obesity (Silver Spring) 19, 500–504.

Stice, E., Spoor, S., Bohon, C., Small, D.M., 2008. Response to food is moderated by TaqIA A1 allele relation between obesity and blunted striatal. Science 322, 449–452.

Szczepanska-Sadowska, E., Cudnoch-Jedrzejewska, A., Ufnal, M., Zera, T., 2010. Brian and cardiovascular diseases: common neurogenic background of cardiovascular, metabolic, and inflammatory diseases. J. Physiol. Pharmacol. 509–521.

Thaler, J.P., Yi, C., Schur, E.A., Guyenet, S.J., Hwang, B.H., Dietrich, M.O., Zhao, X., Sarruf, D.A., Izgur, V., Maravilla, K.R., Nguyen, H.T., Fischer, J.D., Matsen, M.E., Wisse, B.E., Morton, G.J., Horvath, T.L., Baskin, D.G., Tschöp, M.H., Schwartz, M.W., 2012. Obesity is associated with hypothalamic injury in rodents and humans. J. Clin. Invest. 122.

Thurfjell, L., Bengtsson, E., Nordin, B., 1992. A new three-dimensional connected components labeling algorithm with simultaneous object feature extraction capability. CVGIP Graph. Model. Image Process. 54, 357–364.

Uysal, K., Wiesbrock, S., Marino, M., Hotamisligil, G., 1997. Protection from obesity-induced insulin resistance in mice lacking TNF-alpha function. Nature 389, 610–614.

Verstynen, T., Weinstein, A.M., Schneider, W., Jakicic, J., Rofey, D., Erickson, K., 2012. Increased body mass index is associated with a global and distributed decrease in white matter microstructural integrity. Psychosom. Med. 74, 682–690.

Walther, K., Birdsill, A.C., Glisky, E.L., Ryan, L., 2010. Structural brain differences and cognitive functioning related to body mass index in older females. Hum. Brain Mapp. 31, 1052–1064.
Wang, S., Wu, E.X., Tam, C.N., Lau, H.-F., Cheung, P.-T., Khong, P.-L., 2008. Characterization of white matter injury in a hypoxic–ischemic neonatal rat model by diffusion tensor MRI. Stroke 39, 2348–2353.
Watson, G.S., Craft, S., 2006. Insulin resistance, inflammation, and cognition in Alzheimer's disease: lessons for multiple sclerosis. J. Neurol. Sci. 245, 21–33.
Wedeen, V.J., Hagmann, P., Tseng, W.-Y.I., Reese, T.G., Weisskoff, R.M., 2005. Mapping complex tissue architecture with diffusion spectrum magnetic resonance imaging. Magn. Reson. Med. 54, 1377–1386.
Xu, J., Li, Y., Lin, H., Sinha, R., Potenza, M.N., 2011. Body mass index correlates negatively with white matter integrity in the fornix and corpus callosum: a diffusion tensor imaging study. Hum. Brain Mapp. http://dx.doi.org/10.1002/hbm.21491.
Yaffe, K., 2007. Metabolic syndrome and cognitive disorders: is the sum greater than its parts? Alzheimer Dis. Assoc. Disord. 21, 167–171.
Yates, K.F., Sweat, V., Yau, P.L., Turchiano, M.M., Convit, A., 2012. Impact of metabolic syndrome on cognition and brain: a selected review of the literature. Arterioscler. Thromb. Vasc. Biol. 32, 2060–2067.
Yau, P.L., Castro Bs, M.G., Tagani, A., Tsui, W.H., Convit, A., 2012. Obesity and metabolic syndrome and functional and structural brain impairments in adolescence. Pediatrics 130 (4), e856–e864.